Genome-wide scan and fine-mapping of rare nonsynonymous associations implicates intracellular lipolysis genes in fat distribution and cardio-metabolic risk

Luca A. Lotta[a], Liang Dong[b], Chen Li[a], Satish Patel[b], Isobel D. Stewart[a], Koini Lim[b], Felix R. Day[a], Eleanor Wheeler[a], Craig A. Glastonbury[c,d], Marcel Van de Streek[c], Stephen J. Sharp[a], Jian'an Luan[a], Nicholas Bowker[a], Martina Schweiger[e], Laura B. L. Wittemans[a], Nicola D. Kerrison[a], Lina Cai[a], Debora M. E. Lucarelli[a], Inês Barroso[f], Mark I. McCarthy[g,h,i], Robert A. Scott[a], Rudolf Zechner[e], John R. B. Perry[a], Vladimir Saudek[b], Kerrin S. Small[c], Stephen O'Rahilly[b1], Nicholas J. Wareham[a1], David B. Savage[b1], Claudia Langenberg[a1].

a MRC Epidemiology Unit, University of Cambridge School of Clinical Medicine, Box 285 Institute of Metabolic Science, Cambridge Biomedical Campus, Cambridge, United Kingdom, CB2 0QQ
b University of Cambridge Metabolic Research Laboratories, Wellcome Trust-MRC Institute of Metabolic Science, Box 289, Cambridge Biomedical Campus, Cambridge, United Kingdom, CB2 0QQ
c Department of Twin Research and Genetic Epidemiology, King's College London, St Thomas' Campus, Lambeth Palace Road, London, SE1 7EH, United Kingdom
d Big Data Institute, Li Ka Shing Centre for Health Information and Discovery, University of Oxford, Old Road Campus, Oxford, OX3 7LF, United Kingdom
e Institute of Molecular Biosciences, University of Graz, 8010 Graz, Austria
f Wellcome Sanger Institute, Hinxton, Cambridge, CB10 1SA, United Kingdom
g Oxford Centre for Diabetes, Endocrinology and Metabolism, Churchill Hospital, University of Oxford, Headington, Oxford, OX3 7LE, United Kingdom
h Wellcome Centre for Human Genetics, University of Oxford, Roosevelt Drive, Oxford, OX3 7BN United Kingdom
i Oxford NIHR Biomedical Research Centre, Oxford University Hospitals Trust, Headley Way, Headington, Oxford, OX3 9DU, United Kingdom
1 these authors contributed equally

Correspondence to:
Claudia Langenberg (claudia.langenberg@mrc-epid.cam.ac.uk, +44 (0) 1223 330315)
David B. Savage (dbs23@medschl.cam.ac.uk, +44 (0) 1223 767923)
Nicholas J. Wareham (nick.wareham@mrc-epid.cam.ac.uk, +44 (0) 1223 330315)
Stephen O'Rahilly (so104@medschl.cam.ac.uk, +44 (0) 1223 336855)
Luca A. Lotta (luca.lotta@mrc-epid.cam.ac.uk, +44 (0) 1223 330315)

Abstract

Difficulties in identifying causal variants and genes underlying genetic associations have limited the translational potential of genetic studies of body fat distribution, an important, partly-heritable risk factor for cardio-metabolic disease. Rare variant associations facilitate fine-mapping of causal alleles, but their contribution to fat distribution is understudied. We performed a genome-wide scan of rare nonsynonymous variants for body mass index-adjusted waist-to-hip-ratio (BMI-adjusted WHR; a widely-used measure of fat distribution) in 450,562 European ancestry individuals, followed by systematic Bayesian fine-mapping at six genome-wide ($p<5\times10^{-08}$; main-analysis) and two subthreshold signals (significant at a Bonferroni-corrected $p<1.3\times10^{-06}$). We found strong statistical evidence of causal association for nonsynonymous alleles in *CALCRL* (p.L87P, $p_{conditional}=5.9\times10^{-12}$; posterior-probability of association [PPA]=52%), *PLIN1* (p.L90P, $p_{conditional}=5.5\times10^{-13}$; PPA>99%), *PDE3B* (p.R783X, $p_{conditional}=6.2\times10^{-15}$; PPA>99%), *ACVR1C* (p.I195T; $p_{conditional}=5.4\times10^{-12}$; PPA>99%), and *FGF1* (p.G21E, $p_{conditional}=1.6\times10^{-07}$; PPA=98%). Alleles at the four likely-causal main-analysis genes affected fat distribution primarily via larger hip- rather than smaller waist-circumference and six of nine conditionally-independent WHR-lowering index-variants were associated with protection from cardiovascular or metabolic disease. All four genes are expressed in adipose tissue and have been linked with the regulation of intracellular lipolysis, which controls fat retention in mature cells. Targeted follow-up analyses of key intracellular-lipolysis genes revealed associations for a variant in the initiator of intracellular lipolysis *PNPLA2* (p.N252K) with higher BMI-adjusted-WHR and higher cardio-metabolic risk. This study provides human genetic evidence of a link between intracellular lipolysis, fat-distribution and its cardio-metabolic complications in the general population.

Introduction

Body fat distribution is a major risk factor for cardiovascular and metabolic disease independent of obesity (1-5), but the mechanistic foundations of this link are poorly understood. Several common variants associated with fat distribution (6) or with compartmental fat deposition (7, 8) are located in regulatory regions near genes that are highly expressed in adipose tissue. While consistent with a biologically plausible role of adipocyte function in fat distribution, the translational potential of these observations is limited by challenges in inferring causal genes and mechanisms underlying associations of non-coding genetic variants. In contrast, the study of low-frequency nonsynonymous alleles has catalyzed translation from gene identification to therapeutic drug development, as illustrated by associations in *PCSK9* (9, 10), *LPA* (11), *APOC3 (12, 13)* or *ANGPTL3 (14-16)* with lipid phenotypes leading to rapid drug development for cardiovascular prevention (15, 17-22).

Previous genome-wide association studies of fat distribution in ~225,000 people have focused mostly on common variants (6). Rare variants, defined by the 1000 Genomes Project by minor allele frequency (MAF) below 0.5% (23), are usually population-specific (23) and difficult to impute (24), and hence their study requires large, homogeneous samples and direct genotyping. Their contribution to fat distribution remains understudied. A critical advantage of studying rare variants is that they represent mutational events which occurred more recently in a population (23), so that they tend to occur on long haplotypes together with more common variation with which correlation is low (25). This facilitates statistical fine-mapping aimed at identifying causal variants and distinguishing scenarios where the rare variant is causal rather than just a “passenger” in the association signal (25). Causal nonsynonymous variants in a gene provide a strong link between gene and phenotype and also a “genetic model” for functional studies aimed at understanding the underlying mechanism of association.

87 To exploit these properties, we conducted a genome-wide discovery scan of the association
88 of rare nonsynonymous variants with body mass index-adjusted waist-to-hip ratio (BMI-adjusted
89 WHR; a widely-used measure of body fat distribution (5, 6)) in 450,562 European ancestry
90 individuals. We then conducted systematic analyses of genomic context to distinguish likely-
91 causal from non-causal associations. The aim was to identify variants, genes and pathways
92 implicated in the regulation of fat distribution in the general population.

Results

Genome-wide scan of rare nonsynonymous variants and fine-mapping at identified loci

We conducted a genome-wide association scan of 37,435 directly-genotyped, rare (MAF <0.5%) nonsynonymous variants with BMI-adjusted WHR in 450,562 European ancestry participants of UK Biobank (**SI Appendix Notes S1-S2, Tables S1-S2 and Fig. S1**). There was evidence of modest inflation of signal (λ=1.045), consistent with polygenic contributions to BMI-adjusted WHR (**SI Appendix Fig. S2**). In the main analysis, we identified six associations at the genome-wide level of statistical significance ($p<5\times10^{-08}$) in genes at least 1 Mb apart of each other (**SI Appendix Table S3 and Fig. S2**). In addition to the main analysis, we also identified two additional signals in a women-specific analysis ($p<5\times10^{-08}$ in a women-only secondary analysis; **SI Appendix Table S3**) and two additional signals that met a Bonferroni-corrected statistical significance threshold in the sex-combined analysis (experiment-level $p<1.3\times10^{-06}$, i.e. a correction for 37,435 variants tested; **SI Appendix Table S3**).

We conducted systematic analyses of genomic context to establish whether the identified rare nonsynonymous variants are likely to be causal for the association with BMI-adjusted WHR, including conditional analyses and fine-mapping of statistically-decomposed signals (**Methods**). Fine-mapping analyses provided strong statistical evidence for the causal association of rare nonsynonymous variants of *CALCRL*, *PLIN1*, *PDE3B* and *ACVR1C* in the main analysis and of *FGF1* in the experiment-level statistical significance secondary analysis (**Table 1, Fig. 1, and SI Appendix Fig. S3**). Conversely, genomic context analyses were not consistent with causal associations for identified rare nonsynonymous variants in *ABHD15* (main analysis), *PYGM* (main analysis), *PLCB3* (experiment-level statistical significance and women-specific secondary analyses) or *FNIP1* (women-specific secondary analysis; all results in **SI Appendix Tables S3-S4 and Note S3**).

At *CALCRL*, there was evidence of two conditionally-independent signals (**Table 1, Fig. 1, and SI Appendix Table S5**), led by the rs10177093 common variant and by the rare p.L87P variant, respectively. Fine-mapping at the latter signal yielded a 99% credible set including only two variants, rs61739909 (*CALCRL* p.L87P, posterior probability of casual association [PPA]=51%) and rs180960888 (intronic to *CALCRL*, PPA=48.5%). Hence, p.L87P is the most likely causal variant and *CALCRL* the most likely causal gene for this signal. Previous genome-wide association studies had identified an association at this locus led by rs1569135 (6), which is in linkage disequilibrium with the lead common variant for the first signal in this larger analysis (rs10177093; R^2=0.74). However, this association had not been linked to *CALCRL* via fine-mapping nor were nonsynonymous variants in this gene previously associated with any fat distribution phenotypes.

At *PLIN1*, there was evidence of only one signal led by the rare p.L90P variant (**Table 1 and Fig. 1**), which was the only variant in the 99% credible set (PPA>99%; **Table 1**).

At *PDE3B*, there was evidence of three signals, the strongest of which was led by the rs150090666 p.R783X nonsense variant in *PDE3B*, which was the only variant in the 99% credible set (PPA>99%; **Table 1 and Fig. 1**). As part of an analysis focused on predicted loss-of-function variants in unrelated participants UK Biobank, Emdin et al. reported an association of rs150090666 with height and, in follow-up analyses, of a combination of predicted loss-of-function *PDE3B* variants with BMI-adjusted WHR which was below the genome-wide level of significance (26). In that study, the genomic context of the association with height, but not BMI-adjusted WHR, was considered. In this study, we included a larger sample of European ancestry participants (including related individuals) and optimally accounted for relatedness and population substructure using a mixed-model, finding a genome-wide significant association for rs150090666 with BMI-adjusted WHR, with fine-mapping providing the strongest possible

statistical evidence of causal association for this variant.

At *ACVR1C,* there was evidence of three distinct signals (**Table 1 and Fig. 1**). The rare p.I195T variant led one of the secondary signals at this region and was the only variant in the 99% credible set (PPA>99%; **Table 1**). In addition, the primary signal at this region was led by a low-frequency missense variant in *ACVR1C* (rs55920843, p.N150H), which also had the highest posterior probability in fine-mapping of this signal (PPA>99%; **Table 1**). Hence, fine-mapping of conditionally-independent signals at this locus converges on *ACVR1C* as causal gene for body fat distribution and p.I195T and p.N150H as causal variants for the respective association peaks.

Additional consideration of subthreshold-signals that met the experiment-level Bonferroni correction showed evidence of six conditionally-independent signals in and around the *FGF1* gene, one of which was led by the rare p.G21E missense variant (PPA=98%; **Table 1 and SI Appendix Fig. S3**).

Given previous reports of sex-specific associations with BMI-adjusted WHR (6), we estimated stratified associations for likely-causal variants identified in our analysis and, in line with previous studies (6), found larger effect-size estimates in women compared to men, with a statistically-significant difference for rs150090666 p.R783X in *PDE3B* ($p_{heterogeneity}=5.2\times10^{-06}$; **SI Appendix Table S6**).

In a gene-based analysis, the burden of rare nonsynonymous alleles in *PLIN1*, the only gene with other rare nonsynonymous variants in addition to those found in the main analysis, was not associated with statistically-significant differences in BMI-adjusted WHR (**SI Appendix Table S7**).

Functional annotation, structural modelling and associations with cardio-metabolic phenotypes

We conducted detailed *in silico* analyses that predict functional impact of identified variants

(**SI Appendix Box S1 and Table S8**) and estimated their association with a variety of continuous cardio-metabolic traits and outcomes (**Fig. 2-3**), to gain insights into their likely function and phenotypic impact.

Genetic variants can affect fat distribution via increased abdominal fat (larger waist), reduced gluteofemoral fat (smaller hip) or both. The minor alleles of all four rare nonsynonymous variants in *CALCRL, PLIN1, PDE3B,* and *ACVR1C* were associated with lower waist-to-hip ratio (i.e. a more favorable fat distribution) and larger hip circumference, but were not associated with waist circumference (**Fig. 2-3**). Certain genetic variants associated with greater gluteofemoral fat show associations with protection from cardio-metabolic disease, possibly by facilitating storage in more favorable fat depots (7). At the *CALCRL, PLIN1, PDE3B,* and *ACVR1C* loci, two of the four rare nonsynonymous variants and six of nine total conditionally-independent WHR-lowering alleles were associated with protection from type 2 diabetes or coronary artery disease ($p<0.05$; **Fig. 2-3, SI Appendix Table S9**), suggesting that the identified variants may enhance the storage capacity of gluteofemoral adipose tissue. The four rare nonsynonymous variants were also associated with other cardio-metabolic phenotypes (**Fig. 2-3**), as described in more detail below.

The *CALCRL* p.L87P variant was associated with higher high-density lipoprotein cholesterol (HDL-C) and protection from coronary disease (**Fig. 2**). The variant occurs near a strictly conserved disulfide cross-link in this G-protein coupled receptor, but leucine 87 itself is not a conserved residue as it is replaced by proline in several species (**SI Appendix Box S1**), consistent with integrated evidence from sixteen *in silico* prediction algorithms (**SI Appendix Table S8**). This suggests that p.L87P has a mild functional impact on this G-protein coupled receptor the knock-out of which is embryonically-lethal in mice (**SI Appendix Box S1**) (27). The p.L90P variant in *PLIN1*, occurring near the conserved serine 81 which is believed to be involved in the interaction of perilipin 1 with hormone sensitive lipase (**SI Appendix Box S1**), was

associated with higher overall adiposity and lower low-density lipoprotein cholesterol (LDL-C; **Fig. 2**). *In silico* prediction algorithms provide initial evidence of a likely-deleterious impact of this variant (**SI Appendix Table S8**). Loss-of-function mutations in *PLIN1* are associated with autosomal dominant forms of partial lipodystrophy with lack of gluteofemoral and leg fat, insulin resistance, dyslipidemia and type 2 diabetes (**SI Appendix Box S1**) (28). The nonsense p.R783X variant in *PDE3B* results in the premature truncation of phosphodiesterase 3B within its catalytic domain and structural modelling predicts the variant protein to be catalytically dead (**SI Appendix Box S1**). Phosphodiesterase 3B is a membrane-bound phosphodiesterase implicated in terminating intracellular lipolysis in response to insulin (29), hence an inactive enzyme would result in enhanced intracellular lipolysis at the sites where this phosphodiesterase is expressed. The variant was associated with approximately a quarter of a standard deviation lower BMI-adjusted WHR (an effect estimate six times greater than that of the strongest common variants identified in previous genome-wide association studies; **SI Appendix Fig. S4**), higher BMI and fat percentage, but lower blood pressure and lower triglycerides (**Fig. 2**). Nominal associations with protection from physician-diagnosed hypercholesterolemia and coronary artery disease have been reported for predicted loss-of-function variants in this gene (26), showing that loss-of-function of the gene may increase overall adiposity, but have protective associations with other cardio-metabolic traits (i.e. blood pressure, lipid levels, and coronary disease). In light of the statistical evidence for sex-specific association with BMI-adjusted WHR, we estimated associations of p.R783X with diabetes and coronary risk separately in men and women, but did not observe statistically-significant differences in risk for either sex (**SI Appendix Table S10**).

At *ACVR1C*, encoding a negative regulator of the peroxisome proliferator-activated receptor gamma (30), both p.N150H and p.I195T missense variants were associated with lower diastolic blood pressure and protection from type 2 diabetes (**Fig. 3**). On the basis of the three independent

lead variants at this locus (**Table 1**), each standard-deviation genetically-lower BMI-adjusted WHR via *ACVR1C* was associated with a 69% lower risk of type 2 diabetes (odds ratio, 0.31; 95% confidence interval, 0.18 to 0.54; $p=3.1\times10^{-05}$). The p.I195T missense variant, which *in silico* software and structural modelling predict having a more deleterious functional impact than p.N150H (**SI Appendix Box S1 and Table S8**), also had greater phenotypic impact on WHR and diabetes risk (**Fig. 3**). At *FGF1*, we found an association for the rare WHR-lowering p.G21E allele with protection against coronary disease (**SI Appendix Fig. S5).**

Interestingly, all four genes implicated in the main analysis are abundantly expressed in subcutaneous and visceral adipose tissue in GTEx (31) and a review of functional evidence revealed links between each of the four encoded proteins and the regulation of intracellular lipolysis, the pathway responsible for the hydrolysis and release of intracellular fat from within mature cells (**SI Appendix Box S1**). Perilipin 1 and phosphodiesterase 3B are well established negative regulators of intracellular lipolysis (29, 32-34), ACVR1C has been experimentally shown to inhibit intracellular lipolysis in mouse adipocytes (30), while CALCRL is the receptor of adrenomedullin (35), which has been shown to stimulate intracellular lipolysis in human adipocytes (details in **SI Appendix Box S1**). We conducted hypothesis-free pathway-enrichment analyses using the likely-causal genes identified in this study and found evidence of enrichment for intracellular lipolysis genes ($p_{pathway\text{-}enrichment}=0.00093$; **SI Appendix Table S11**), in addition to insulin-receptor related signaling pathways, which are established casual pathways in extreme and less severe forms of lipodystrophy (7, 36).

Additional evidence of genetic associations at intracellular lipolysis genes

These data led us to hypothesize that variants at enzymes catalyzing the three hydrolytic reactions of intracellular lipolysis or at their direct regulators might affect fat distribution (**Fig. 4**). To test this hypothesis, we performed targeted follow-up association analyses of all genetic variation within regions 1 Mb either side of five key genes regulating each of the three hydrolytic reactions in the pathway and also estimated associations of the burden of rare nonsynonymous variants in these genes (**Methods**). While there were no associations at *G0S2* or *LIPE*, there were strong associations at *MGLL*, *ABHD5* and *PNPLA2* ($p<5\times10^{-08}$). At *MGLL* and *ABHD5* the link between genetic associations and these lipolysis genes were unclear. The association at *MGLL* was in the shadow of an association peak over 2 Mb downstream of the gene, which was greatly attenuated after conditioning for the index-variants, suggesting that this signal is unlikely to be via this gene (**SI Appendix Fig. S6 and Table S12**). At *ABHD5*, there was evidence for one association peak led by a synonymous variant in the gene (rs141365045; **SI Appendix Table S13 and Fig. S7**), which tags a low-frequency haplotype spanning the entire gene. The 99% credible set at this association signal comprises 42 variants in this haplotype that evenly share the PPA (PPA range 0.7%-3.3%), suggesting that any or a combination of these variants could be causal. The haplotype does not encompass nonsynonymous variants in the gene and the lead rs141365045 is associated with expression of the nearby *ANO10* and *SNRK-AS1* in thyroid tissue, but not *ABHD5* in GTEx (31).

We identified an association in *PNPLA2*, encoding adipose triglyceride lipase (ATGL) which is the enzyme responsible for the initiation of intracellular lipolysis (37) (**Fig. 4**). At the locus, there was evidence of two independent signals the strongest of which was led by a missense variant occurring near a splice-site junction in the gene (rs140201358-G p.N252K; MAF=1.4%; beta in standard deviations of BMI-adjusted WHR per minor allele [252K], 0.08; standard error,

0.009; $p=2.5\times10^{-22}$; **SI Appendix Table S13 and Fig. S7**). Associations were similarly strong in men and women ($p_{heterogeneity}=0.10$; **SI Appendix Table S6**). Fine-mapping of the main signal in the region identified rs140201358 as the only variant in the 99% credible set, supporting a likely-causal association (PPA>99%; **SI Appendix Table S13 and Fig. S7**).

Follow-up analyses of the rs140201358-G p.N252K variant showed associations with lower BMI and smaller hip circumference, but higher triglycerides and LDL-C (**Fig. 5A**). Disease outcome association analyses revealed an association with higher risk of type 2 diabetes (odds ratio per 252K allele, 1.09; 95% confidence interval, 1.02-1.17; p=0.0073) and coronary artery disease (odds ratio per 252K allele, 1.12; 95% confidence interval, 1.04-1.20; p=0.0019; **Fig. 5B**).

We conducted a number of *in vitro* experiments to provide an initial functional characterization of the possible mechanisms linking rs140201358 with fat distribution. *In vitro* experiments showed similar basal-, ABHD5 stimulated- and GOS2-inhibited enzyme activity as well as similar localization to lipid droplets between PNPLA2-N252K and wild-type PNPLA2 (**Fig. 5C and SI Appendix Fig. S8**), in keeping with structural modelling (**SI Appendix Box S1**). However, the C>G substitution occurs at position -2 at the donor splice site of exon 6 in a partially-conserved nucleotide that is never substituted with a G in mammalian species, suggesting a possible impact on splicing (**Fig. 5D**). *In silico* software predicted this change to result in the creation of an exonic splicing silencer site, with higher probability of exon skipping (**Methods**). We hypothesized that if the variant affected the correct splicing of *PNPLA2*, this could alter allele-specific expression of *PNPLA2* in carriers. To assess this, we investigated the allele-specific expression of *PNPLA2* in subcutaneous adipose tissue from four unrelated heterozygous carriers of rs140201358-G from the Twins UK study. Across the four carriers, there were 2,032 reads of *PNPLA2* mRNA in subcutaneous adipose tissue. The number of reads

carrying the alternative G allele (i.e. 252K) was 21% lower than that of reads containing the wild-type C allele (observed reads, 900; expected, 1,016; two-tailed binomial $p=2.9\times10^{-07}$), with a statistically-significant within-individual difference in three out of four carriers ($p<0.05$; **Fig. 5E**). To assess impact on overall expression, we conducted quantitative polymerase chain reaction (Q-PCR) analyses of *PNPLA2* expression in peripheral blood mononuclear cells from 106 homozygous carriers of the wild-type C allele and 26 heterozygous carriers of the alternative G allele from the Fenland study. Heterozygous carriers of the G allele had 0.39 standard deviations lower overall levels of *PNPLA2* mRNA compared to homozygous wild-type individuals (beta in standard deviations, -0.39; standard error, 0.15; p=0.011; **Fig. 5F**). It remains to be established if associations with expression levels do reflect a splicing defect or result from other regulatory mechanisms due to rs140201358 or correlated variants.

In gene-based analyses, the one rare nonsynonymous variant in *PNPLA2* captured by genotyping (p.S407F) or 10 rare variants in the other intracellular lipolysis genes were not associated with statistically-significant differences in BMI-adjusted WHR (**SI Appendix Table S7**).

297 **Discussion**

298 By combining human genetics studies in over half a million people with *in silico* and *in vitro*
299 functional analyses, we found evidence implicating intracellular lipolysis genes in the regulation
300 of fat distribution and its cardio-metabolic consequences in the general population. This genetic
301 study focused on a subset of genetic variation in order to maximize translational insights of
302 genetic findings and is distinct from but complementary to genome-wide association studies
303 assessing all genetic variants to clarify the overall genetic architecture of a trait. In addition,
304 given the strict criteria for statistical significance and the systematic analysis of genomic context,
305 all of the likely-causal alleles found in the main analysis would meet the strictest statistical
306 significance thresholds recommended for genome-wide analyses of densely genotyped or
307 imputed datasets, including those appropriate for the analysis of whole genome sequencing
308 results (38). By identifying nonsynonymous alleles with high probability of being the causal
309 variants underlying identified associations, this study provides (a) new and specific insights that
310 go beyond the general notion of an impact of adipocyte function on body fat distribution and (b)
311 a basis for the understanding of the molecular mechanisms behind these robust phenotypic
312 associations. With fine-mapping, we show that five nonsynonymous variants at four of the
313 identified genes (*PLIN1*, *PDE3B*, *ACVR1C*, and *PNPLA2*, found via targeted follow-up analysis)
314 had >99% PPA, the highest possible statistical evidence of causal association.

315 Studies in rare forms of human lipodystrophy (36, 39), in experimental models (40-42) and
316 recently also in the general population (7, 43-45) have implicated an impaired capacity to store
317 fat in peripheral adipose compartments in cardio-metabolic disease. Our results highlight
318 intracellular lipolysis as a novel mechanism linking impaired peripheral fat deposition to the risk
319 of cardio-metabolic disease. Intracellular lipolysis is the biochemical process that regulates the
320 release of fatty acid molecules from mature cells and its level of activation ultimately controls the

propensity of peripheral adipocytes, and other tissues, to retain energy stores in the form of fat (46, 47). Therefore, modulating this pathway determines where and how efficiently surplus energy is stored and thus the risk of the complications of sustained positive energy balance. In addition, in a secondary analysis of this study we found evidence of a likely-causal association with lower BMI-adjusted WHR of a rare missense variant in *FGF1*, a gene that murine experiments have implicated in the remodeling of adipose tissue in response to fluctuations in nutrient availability (48). In addition to previous evidence about the role of adipogenesis and intravascular lipolysis (7), findings from this study around intracellular lipolysis and the FGF1-pathway highlight the importance of adipose tissue plasticity in response to energy availability as a critical mechanism in the determination of fat distribution and its cardio-metabolic consequences.

All four likely-causal genes identified in our hypothesis-free main-analysis of rare, nonsynonymous variants have been implicated in intracellular lipolysis by orthogonal experimental evidence. In addition, a missense variant in *PNPLA2*, encoding the initiator of intracellular triglyceride hydrolysis, was associated with unfavorable fat distribution, higher atherogenic lipid levels and higher risk of type 2 diabetes and coronary artery disease further supporting the main findings from the scan of rare variants. Rare loss-of-function mutations in *PNPLA2* cause a recessively-inherited lipid storage disease characterized by ectopic fat deposition, known as neutral lipid storage disease with myopathy, which in some of the few reported cases has been associated with dyslipidemia and diabetes (49-52). Our study is consistent with a role of intracellular lipolysis genes in the aetiology of cardiovascular and metabolic disease in the general population, in line with an earlier study of the Amish population suggesting that a deletion in hormone sensitive lipase (*LIPE*), present in ~5% of Amish people but rarely detected in other populations, results in lower intracellular lipolysis, smaller

adipocytes, insulin resistance and higher diabetes risk (53).

Intracellular lipolysis is a pharmacologically modifiable pathway. The gene products of *ACVR1C* and *PNPLA2* have generated interest as potential drug targets for obesity and its complications (30, 54-57) on the basis of mouse models showing lower fat accumulation and improved glucose metabolism upon downregulation or pharmacologic inhibition of these proteins. In our human genetic studies, the peripheral adiposity-increasing alleles at these genes were associated with protection from diabetes (*ACVR1C* and *PNPLA2*) and coronary disease (*PNPLA2*). Hence, pharmacologically enhancing and not reducing peripheral fat deposition by modulating these genes could protect from cardio-metabolic disease in humans. In addition, the product of *PDE3B* is inhibited by cilostazol, a non-selective inhibitor of both phosphodiesterase 3B and 3A used in cardiovascular medicine for its anti-platelet and vasodilating properties (58, 59). The interaction between PLIN1 and ABHD5 can also be inhibited pharmacologically, resulting in enhanced PNPLA2 activity (60). The association of variation in intracellular lipolysis genes with multiple cardio-metabolic risk factors and outcomes in our study provides human genetic evidence supporting further pharmacological development for this pathway. Also, the translational implications of the association of the *FGF1* p.G21E missense variant with fat distribution and protection from coronary disease deserve further exploration in light of the mounting therapeutic interest around this pathway (61, 62).

In conclusion, our study provides human genetic evidence of a link between genes involved in the regulation of intracellular lipolysis, fat-distribution and its cardio-metabolic complications in the general population.

Methods

Study design and rationale

The aim of this study was to identify likely-causal nonsynonymous genetic variants and genes implicated in the regulation of body fat distribution. We performed a hypothesis-free genome-wide scan of rare (MAF<0.5% in keeping with the 1000 Genomes Project definition (23)) nonsynonymous variants coupled with systematic conditional and fine-mapping analyses at identified loci. We focused on rare variants because (a) they facilitate fine-mapping approaches for causal variant identification (25) and (b) their contribution to fat distribution is understudied (6). Since these variants are usually population-specific (23) and difficult to impute (24), their study requires large, homogeneous samples and direct genotyping. For these reasons, we focused on variants that were directly-genotyped by array genotyping in a single, large population-based cohort, the UK Biobank study (63). Analyses were focused on individuals of European ancestry. We chose to focus on nonsynonymous variation as (a) disease-associated variants are enriched for nonsynonymous variants (38), (b) if a causal variant is a nonsynonymous variant in a gene, this provides strong evidence for the causal role of the gene (64) and (c) the identification of causal nonsynonymous variants facilitates downstream functional analyses aimed at understanding the underlying mechanisms of association. An overview of the study design is in **SI Appendix Fig. S1**.

Main and secondary analyses

In the main analysis, we studied associations of rare (MAF<0.5%) nonsynonymous variants with BMI-adjusted WHR in a sex-combined analysis of 452,302 people using the conventional threshold of genome-wide statistical significance ($p<5\times10^{-08}$). In secondary analyses, we further considered (a) subthreshold associations with BMI-adjusted WHR that met an experiment-level

391 statistical significance threshold ($p<1.3\times10^{-06}$; corresponding to a Bonferroni correction for
392 37,435 tested genetic variants) or (b) genome-wide significant associations ($p<5\times10^{-08}$) in sex-
393 specific analyses in men or women-only.
394
395 *Studies and participants*
396 Genetic analyses were conducted in up to 452,302 European ancestry participants of UK
397 Biobank who underwent genome-wide genotyping (**SI Appendix Table S2**). UK Biobank is a
398 population-based cohort of 500,000 people aged between 40-69 years who were recruited in
399 2006-2010 from centers across the United Kingdom (63). In UK Biobank, waist and hip
400 circumference were measured using a Seca 200cm tape measure, height was measured using a
401 Seca 240cm measure, while weight and body fat percentage were measured using a Tanita
402 BC418MA body composition analyzer
403 (https://biobank.ctsu.ox.ac.uk/crystal/docs/Anthropometry.pdf). Blood pressure and resting heart
404 rate were measured using an Omron blood pressure monitor following a standardized procedure
405 (http://biobank.ctsu.ox.ac.uk/crystal/docs/Bloodpressure.pdf). Type 2 diabetes was defined on the
406 basis of self-reported physician diagnosis at nurse interview or digital questionnaire, age at
407 diagnosis > 36 years, use of oral anti-diabetic medications and electronic health records (65).
408 Coronary artery disease was defined as either (a) myocardial infarction or coronary disease in the
409 participant's medical history documented by a trained nurse at the time of enrolment or (b)
410 hospitalization or death involving acute myocardial infarction or its complications (i.e.
411 International Statistical Classification of Diseases and Related Health Problems codes I21, I22 or
412 I23), consistent with previous work (66, 67).
413 In addition to UK Biobank, genetic associations with type 2 diabetes were estimated from the
414 EPIC-InterAct study (68) and the DIAbetes Genetics Replication And Meta-analysis (69)

(DIAGRAM), with a maximum sample size of 47,008 cases and 492,962 controls. In addition to UK Biobank, genetic associations with coronary artery disease were estimated from the CARDIoGRAMplusC4D consortium (70), with a maximum sample size of 85,358 cases and 551,249 controls. Lipid traits associations were from up to 304,873 participants of the Global Lipids Genetics Consortium (71, 72). Associations with lipid traits for the p.R783X variant in *PDE3B*, which was not studied in the Global Lipids Genetics Consortium, were estimated in a meta-analysis of genetic associations in the Fenland (73), EPIC-Norfolk cohorts (74) and EPIC-InterAct subcohort (68). Descriptions of the cohorts participating in each analysis and of the sources of data are presented in **SI Appendix Table S1 and Note S1.** Ethical approvals were obtained at each study site and informed consent was obtained from all participants.

Genome-wide association scan of rare nonsynonymous genetic variants

Similar to previous genetic studies (1, 5, 6), the BMI-adjusted WHR phenotype was constructed as the ratio of waist and hip circumferences adjusted for age, age^2 and BMI. Residuals were calculated for men and women separately and then transformed by the inverse standard normal function. Adjustment for BMI has been suggested to possibly result in spurious associations with higher BMI-adjusted WHR of variants primarily associated with lower BMI (via collider bias) (75). However, likely-causal nonsynonymous variants at *CALCRL*, *PLIN1*, *PDE3B*, *ACVR1C*, *FGF1* and *PNPLA2*, were all also strongly associated with WHR not adjusted for BMI, with stronger associations than with BMI, consistent with a genuine and primary association with fat distribution (**Fig. 2-3, 5A and SI Appendix Fig. S5**). Genetic variants were genotyped in UK Biobank using the Affymetrix UK BiLEVE or the Affymetrix UK Biobank Axiom arrays (76). Genotyping underwent quality control procedures including (a) routine quality checks carried out during the process of sample retrieval, DNA extraction, and genotype

calling; (b) checks and filters for genotype batch effects, plate effects, departures from Hardy-Weinberg equilibrium, sex effects, array effects, and discordance across control replicates; (c) individual and genetic variant call rate filters (76). We further excluded genetic variants with a genotype call rate below 95% and variants that were not rare or nonsynonymous. A total of 37,435 genetic variants in 12,355 genes were available for analysis. Genomic annotations were performed using the Annovar software (77). Genome-wide association analyses in 450,562 participants of European Ancestry were conducted using the BOLT-LMM software (78). BOLT-LMM fits linear mixed models that account for relatedness between individuals using a genomic relationship matrix, adjusting for relatedness and population stratification (78). Full details of these genetic analyses are in **SI Appendix Note S2**.

Conditional analyses and fine-mapping

At each associated genomic region, we conducted systematic analyses of the genomic context of associations. Our goal was to establish whether or not the identified rare nonsynonymous variants are likely to be the causal variants for the association with BMI-adjusted WHR. At each region 1 Mb either side of the nonsynonymous genetic variants associated with BMI-adjusted WHR, we conducted both approximate and formal conditional analyses. We considered the association of all genetic variants in the regions regardless of functional annotation or allele frequency using directly-genotyped and densely-imputed data using the Haplotype Reference Consortium. First, approximate conditional analyses were conducted on summary-level estimates using GCTA (79) to identify sets of conditionally-independent index genetic variants ($p<5\times10^{-08}$ in the main or in sex-specific analyses and $p<1.3\times10^{-06}$ in analyses using experiment-level statistical significance). Individual-level genotypes for the conditionally-independent variants identified in this first step were then extracted in 350,721 unrelated European ancestry

participants of UK Biobank and their independent association was confirmed in multivariable linear regression models including all variants put forward from approximate analyses. Then, at each region, we statistically decomposed the identified index signals by conditioning for the other conditionally-independent index variants. We then performed Bayesian fine-mapping (80) to estimate the posterior probability of association for each variant (PPA, where 0% indicates that the variant is not causal and 100% indicates the highest possible posterior probability that the variant is causal) and define the 99% credible set at that signal (i.e. a set of variants in a genomic window that accounts for 99% of the PPA at that association signal). To perform credible set mapping, the association results at each locus were converted to Bayes factors (BF) for each variant within the locus boundary. The posterior probability that a variant-j was causal was defined by:

$$\varphi j = \frac{BFj}{\Sigma k\, BFk}$$

where, BFj denotes the BF for the jth variant, and the denominator is the sum of BFs for all included variants at that signal. A 99% credible set of variants was created by ranking the posterior probabilities from highest to lowest and summing them until the cumulative posterior probability exceeded 0.99 (i.e. 99%).

Additional associations with BMI-adjusted WHR at intracellular lipolysis regulators

The findings from our rare-variant scan led us to hypothesize that variation at key enzymes of the intracellular lipolytic pathway might affect fat distribution (**Fig. 4**). To test this hypothesis, we systematically investigated variation in and around the key regulators of each of the three enzymatic reactions in intracellular lipolysis (46): *PNPLA2*, *ABHD5*, *G0S2*, *LIPE*, and *MGLL*. *PNPLA2* encodes adipose triglyceride lipase (PNPLA2 or ATGL), the main enzyme for

485 triglyceride hydrolysis; *ABHD5* encodes Alpha-Beta Hydrolase Domain Containing 5 also known
486 as Comparative Gene Identification-58 (CGI-58), the activator of PNPLA2; *G0S2* encodes
487 G0/G1 Switch 2, the inhibitor of PNPLA2; *LIPE* encodes hormone sensitive lipase, the main
488 enzyme for diglyceride hydrolysis; *MGLL* encodes monoglyceride lipase, the main enzyme for
489 monoacylglyceride hydrolysis. For each of these gene regions we estimated their associations
490 with BMI-adjusted WHR for all variants that were either directly genotyped or imputed using the
491 Haplotype Reference Consortium in the region defined by 1 Mb either side of the gene
492 boundaries.
493
494 *Gene-based analyses*
495 For the four likely-causal genes identified in the main analysis (*CALCRL, PLIN1, PDE3B*
496 and *ACVR1C*) and the five key intracellular lipolysis genes (*ABHD5, G0S2, PNPLA2, LIPE* and
497 *MGLL*) we sought to estimate the association with BMI-adjusted WHR of the burden of rare
498 nonsynonymous variants. We extracted genotypes of independent (R^2<0.01) rare nonsynonymous
499 variants in 350,721 unrelated European ancestry participants of UK Biobank with available BMI-
500 adjusted WHR and estimated the burden of these variants using linear regression adjusted for age,
501 sex and genetic principal components comparing carriers to non-carriers of these rare alleles.
502
503 *Structural modelling, functional prediction of identified nonsynonymous variants, pathway*
504 *enrichment analyses*
505 Models were built with the MODELLER software (81). Sequence alignment was achieved
506 by HHpred, MUSCLE and Blast algorithms implemented in MPI toolkit (82). Paralogues and
507 orthologues were extracted from Orthologous Matrix database (83), and displayed and edited in

Jalview (84). Structures are displayed using MolSoft Browser-Pro software (URL: http://www.molsoft.com/icm_browser_pro.html).

We used the Annovar (77) to generate annotations that predict deleteriousness of amino acid changes. We generated the summary results of sixteen computational algorithms that predict whether or not an amino acid change is likely to be deleterious to the function of the encoded protein. For each of these algorithms, the prediction of likely functional impact contributed to an overall score of predicted deleteriousness (see **SI Appendix Table S8** for details on the algorithms and scoring criteria).

We investigated the expression of the likely-causal genes in 53 tissues from the Genotype-Tissue Expression (GTEx) consortium (31). Data were accessed from the online portal (URL: https://www.gtexportal.org/home/) on the 1st of September 2017.

We performed pathway enrichment analyses using the ConsensusPathDB software (http://cpdb.molgen.mpg.de/) (85). The software integrates data from 32 public databases to identify pathways that are over-represented in a given gene list, providing a p-value for enrichment compared to what expected by chance given the number of genes in the list and the prevalence of genes of a given pathway in the list of interrogated genes (in this case the list of 12,355 genes available for analysis).

526 *Initial functional characterization of the PNPLA2 p.N252K variant*

527 Given the central role of *PNPLA2* in intracellular lipolysis and the existence of established
528 experimental protocols for studying the impact of variants of this gene on hydrolytic activity
529 (86), we investigated the impact of the p.N252K variant. Green monkey kidney (Cos-7, ATCC
530 and CRL-165) cells were seeded at 900,000 cells per 10 cm dish and transfected with: (a) human
531 wild-type PNPLA2 tagged with yellow fluorescent protein, (b) human PNPLA2-N252K, and (c)
532 LacZ as a control using Metafectene. Twenty-eight hours after transfection, cells were harvested
533 in 300 µL HSL-buffer plus pi and disrupted by sonication. After centrifugation at 2000 g for 10
534 minutes at 4°C, protein concentration was determined using Bradford reagent and bovine serum
535 albumin as a standard. Expression of human wild-type PNPLA2 and human PNPLA2-N252K
536 was verified by Western Blotting analysis. Triglyceride hydrolase activity assay was performed
537 as described previously (87). A total of 20 µg of Cos-7 lysates containing overexpressed human
538 wild-type PNPLA2, human PNPLA2-N252K or LacZ as a control were incubated with 1µg
539 purified CGI-58 (ABHD5) or 1.5 µg purified G0S2 and radiolabeled Triolein emulsified with
540 PC/PI (0.5 mM, 20 µCi/µmol) for one hour at 37°C. Radioactivity present in the extracted fatty
541 acids was determined using liquid scintillation counting. Activity was measured in three technical
542 replicates, has been corrected for Cos-7 background activity (LacZ) and is presented as mean and
543 individual results of three technical replicates.

544 We also investigated the intracellular localization of wild-type and mutant PNPLA2. Cos-7
545 cells were seeded onto coverslips in 12 well tissue culture plates with a density of 60,000 cells
546 per well and transfected with the following constructs: (a) human wild-type PNPLA2 tagged with
547 yellow fluorescent protein, (b) human PNPLA2-N252K, (c) human PNPLA2-S47A, which is a
548 catalytically inactive variant, (d) human PNPLA2 with both the N252K and S47A variants.
549 Constructs were generated by site-directed mutagenesis using the Agilent primer design software

and the QuickChangeII XL Kit following manufacturer's instructions. 400 µM oleic acid conjugated with BSA was supplemented 4 hours after transfection for 20 hours to promote lipid droplet formation. Cells were fixed with 4% formaldehyde for 15 minutes, followed by three washes in PBS, and incubated with LipidTox DeepRed 633 for 1 hour for lipid droplet staining. Cells were mounted on microscope slides with ProLong Gold Antifade Mountant and the yellow fluorescent protein-tagged PNPLA2 localization was determined using the Leica TCS SP8 confocal microscope with a 63X immersion oil objective (1.3 NA). Yellow fluorescent protein fluorescence was excited at 514 nm and emission was detected between 520 and 545 nm. LipidTox DeepRed was excited at 633 nm and detected between 640–680 nm.

The expression of yellow fluorescent protein-PNPLA2 transfected into Cos-7 cells was determined by immunoblotting as previously described (33, 86). Briefly, cells were rinsed twice with ice-cold PBS and lysed in RIPA buffer supplemented with protease inhibitors. Cell debris was spun down at 13,000 RPM for 10 minutes at 4C. Typically, 15-20 µg of the clarified lysate was resolved and transferred onto nitrocellulose membrane using the NuPAGE Bis-tris SDS PAGE/IBlot system (Invitrogen) with yellow fluorescent protein tagged-PNPLA2 being detected using an anti-GFP antibody (Roche) and GAPDH (GeneTex) serving as loading control.

Impact of the rs140201358-G PNPLA2 variant on gene expression

Splicing consequences for the *rs140201358-G* variant were predicted using the Human Splicing Finder software (88), while the likelihood of exon skipping was predicted using the EX-SKIP software (89).

Allele-specific expression of *PNPLA2* in adipose tissue was investigated in four unrelated heterozygous carriers from 477 female participants of the TwinsUK cohort using paired whole genome sequence and RNAseq data. Phased whole-genome sequence (6X) was generated as

574 described in the UK10K project (90). RNAseq data from subcutaneous adipose tissue was
575 generated as described in Buil and colleagues (91). Raw RNA reads were aligned to personal
576 genomes using the following strategy. The phased whole genome sequences from UK10K were
577 re-aligned to the human genome build GRCh37/hg37 to create diploid personal genomes for each
578 sample using vcf2diploid (92). RNAseq reads were processed as follows. Adapter sequences
579 were trimmed from RNA-seq reads using TrimGalore, software that combines Cutadapt (93) and
580 FastQC (URL: https://www.bioinformatics.babraham.ac.uk/projects/fastqc/). Trimmed sequences
581 with less than 20 bases or which had Phred score below 1 were excluded. Poly-A tails longer than
582 4bp were trimmed with PRINSEQ-lite (94). Processed reads were then aligned to the
583 corresponding personal diploid genomes using Spliced Transcripts Alignment to a Reference
584 (STAR) (95). Pairing of RNA-seq reads was evaluated for a Mapping Quality (MAPQ) score
585 above 30 and a maximum mismatch threshold of 5. Genomic locations of the reads of personal
586 genomes were crosslinked to their genome locations on the reference genome with CrossMap
587 v.0.2.3 (96). A read's haplotype origin was assigned to either the haplotype with the least number
588 of mismatches or assigned randomly to break ties. Uniquely mapped reads were retained and the
589 number of reads mapping to each haplotype was quantified with ASEReadCounter (97). We
590 tested for differential expression of the two alleles of rs140201358 (C or G) in individual carriers
591 and in pooled data from four unrelated carriers by calculating the two-sided bionomial probability
592 of observed reads mapping to the G allele assuming an expected probability of 0.5.

593 Peripheral blood mononuclear cells (PBMCs) were isolated from 1,084 participants of the
594 population based Fenland study (7, 73) using Ficoll-Paque (VWR International Ldt) gradient
595 centrifugation from 20 mL sodium citrate whole blood. After washing with DPBS (Sigma-
596 Aldrich Co Ltd), cells were re-suspended in 1 mL KOSR/DMSO (Sigma-Aldrich Co Ltd) at a
597 concentration of approximately 1×10^7 cells/mL. Vials were frozen to -80 °C in a controlled

container and then transferred to liquid nitrogen. Expression of *PNPLA2* was measured by quantitative polymerase chain reaction (Q-PCR) in 26 heterozygous carriers of the alternative G allele, constituting all carriers with available PBMCs, and a random selection of 106 homozygous carriers of the wild-type C allele. Briefly, RNA was extracted from 1-2 million PBMCs using the RNeasy Plus Micro Kit (Qiagen), following the manufacturer's protocol. A total of 0.1 µg RNA was reverse transcribed to cDNA using M-MLV reverse transcriptase (Promega). Q-PCR was performed to determine the mRNA expression levels of *PNPLA2* and housekeeping gene hypoxanthine phosphoribosyltransferase 1 (*HPRT1*) from undiluted cDNA with TaqMan gene expression assays (ThermoFisher Scientific, Hs00386101_m1 and Hs02800695_m1, respectively), and TaqMan Universal PCR Master Mix. The mRNA expression of *PNPLA2* from each PBMC was normalized to *HPRT1* expression using a standard curve. Measures were carried out in two technical replicates. *PNPLA2* mRNA levels were standardized to a mean of 0 and a standard deviation of 1 using the distribution in wild-type homozygous carriers. The association of genotype status with *PNPLA2* mRNA levels was estimated using repeated measures general linear regression to account for duplicate measures.

Statistical analysis

Genetic associations were estimated using linear mixed models, linear regression or logistic regression as appropriate for the outcome phenotype and study design. Results were scaled to represent the beta estimate in standardized units for continuous outcomes or the odds ratio for binary outcomes per allele. At the *ACVR1C* gene, associations of genetically-determined body fat distribution with type 2 diabetes of multiple genetic variants were estimated using an inverse variance weighted approach (98). Estimates of (1) *ACVR1C* genetic variant to BMI-adjusted WHR and (2) *ACVR1C* genetic variant to diabetes associations were used to calculate estimates

of (3) genetically-higher BMI-adjusted WHR via *ACVR1C* to diabetes association. Statistical analyses were conducted using BOLT-LMM (78) and STATA v14.2 (StataCorp, College Station, Texas 77845 USA).

Data availability

This research has been conducted using the UK Biobank resource. Access to the UK Biobank genotype and phenotype data is open to all approved health researchers (http://www.ukbiobank.ac.uk/).

Data download:
DIAGRAM consortium (http://diagram-consortium.org/)
CARDIoGRAMplusC4D (http://www.cardiogramplusc4d.org/)
GLGC consortium (http://csg.sph.umich.edu//abecasis/public/lipids2013/;
http://csg.sph.umich.edu//abecasis/public/lipids2017/)

Study websites:
UK Biobank (http://www.ukbiobank.ac.uk/)
EPIC-InterAct (http://www.inter-act.eu/)
Twins UK (http://www.twinsuk.ac.uk/)
Fenland (http://www.mrc-epid.cam.ac.uk/research/studies/fenland/)
EPIC-Norfolk (http://www.srl.cam.ac.uk/epic/)

Online data or software:
Human Splicing Finder (http://www.umd.be/HSF3/)
EX-SKIP (http://ex-skip.img.cas.cz/)
FastQC (https://www.bioinformatics.babraham.ac.uk/projects/fastqc/)
MolSoft Browser-Pro (http://www.molsoft.com/icm_browser_pro.html)
ConsensusPathDB (http://cpdb.molgen.mpg.de/)
Genotype-Tissue Expression (GTEx) consortium (https://www.gtexportal.org/home/)

Acknowledgement

This research has been conducted using the UK Biobank resource. Access to the UK Biobank genotype and phenotype data is open to all approved health researchers (http://www.ukbiobank.ac.uk/). This study was funded by the United Kingdom's Medical Research Council through grants MC_UU_12015/1, MC_PC_13046, MC_PC_13048 and MR/L00002/1. This work was supported by the MRC Metabolic Diseases Unit (MC_UU_12012/5) and the Cambridge NIHR Biomedical Research Centre and EU/EFPIA Innovative Medicines Initiative Joint Undertaking (EMIF grant: 115372). Data from the EPIC-InterAct study contributed to this study. EPIC-InterAct Study funding: funding for the InterAct project was provided by the EU FP6 programme (grant number LSHM_CT_2006_037197). D.B.S. and S.O'R. are supported by the Wellcome Trust (WT107064 and WT 095515 respectively) the MRC Metabolic Disease Unit, the National Institute for Health Research (NIHR) Cambridge Biomedical Research Centre and the NIHR Rare Disease Translational Research Collaboration. K.S.S. is supported by MRC Project Grant L01999X/1. The TwinsUK study was funded by the Wellcome Trust and European Community's Seventh Framework Programme (FP7/2007-2013). The TwinsUK study also receives support from the National Institute for Health Research (NIHR)- funded BioResource, Clinical Research Facility and Biomedical Research Centre based at Guy's and St Thomas' NHS Foundation Trust in partnership with King's College London. Some computation was enabled through access granted to K.S.S. to the MRC eMedLab Medical Bioinformatics infrastructure, supported by the Medical Research Council (grant number MR/L016311/1). M. I. McC. is a Wellcome Senior Investigator supported by Wellcome grants 098381, 090532, 106130, 203141. M. I. McC. was supported by the National Institute for Health Research (NIHR) Oxford Biomedical Research Centre (BRC) and the views expressed in this article are those of the author(s) and not necessarily those of the NHS, the NIHR, or the Department of Health. Dr. R. A. S. is an employee and shareholder of GlaxoSmithKline Plc. (GSK). The authors gratefully acknowledge the help of the MRC Epidemiology Unit Support Teams, including Field, Laboratory and Data Management Teams.

Tables

Table 1. Conditionally independent index variants and fine-mapping at the *CALCRL, PLIN1, PDE3B, ACVR1C* and *FGF1* loci.

Locus	Signal	dbSNP rsID	Genomic coordinate, chromosome, position, effect allele, other allele (effect allele frequency, %)	Annotation	Beta (SE) from univariate analysis, in SD units	p-value univariate analysis	Beta (SE) from conditional analysis*, in SD units	p-value conditional analysis*	Genomic position of 99% credible set window, (width in number of base pairs)	Number of variants in the credible set	PPA for the index variant, %
Main analysis											
CALCRL	1	rs10177093	chr2:188213819:G:T (45.6%)	*CALCRL* intronic	-0.02 (0.002)	2.2×10^{-27}	-0.02 (0.002)	7.7×10^{-26}	188088527-188213819 (125,293)	60	17%
	2‡	rs61739909	chr2:188245439:G:A (0.3%)	*CALCRL* p.L87P	-0.13 (0.018)	2.0×10^{-13}	-0.12 (0.018)	5.9×10^{-12}	188245439-188270259 (24,821)	2	51%
PLIN1	1‡	rs139271800	chr15:90214777:G:A (0.1%)	*PLIN1* p.L90P	-0.21 (0.029)	5.5×10^{-13}	-0.21 (0.029)	5.5×10^{-13}	90214777 (1)	1	>99%
PDE3B	1‡	rs150090666	chr11:14865399:T:C (0.1%)	*PDE3B* p.R783X	-0.26 (0.032)	1.4×10^{-15}	-0.25 (0.032)	6.2×10^{-15}	14865399 (1)	1	>99%
	2	rs2970332	chr11:14360435:G:A (23.1%)	*RRAS2* intronic	-0.02 (0.002)	9.9×10^{-12}	-0.02 (0.002)	6.3×10^{-12}	14258010-14689340 (431,331)	20	23%
	3	rs79634051	chr11:14561945:C:G (2.8%)	*PSMA1* intronic	-0.03 (0.006)	6.4×10^{-08}	-0.04 (0.006)	2.1×10^{-09}	14242862-14891141 (648,280)	15	78%
ACVR1C	1	rs55920843	chr2:158412701:G:T (1.2%)	*ACVR1C* p.N150H	-0.08 (0.009)	8.9×10^{-19}	-0.09 (0.009)	4.6×10^{-20}	158412701 (1)	1	>99%
	2	rs2444770	chr2:158503739:C:T (14.8%)	18kb 5' of *ACVR1C*	-0.02 (0.003)	5.9×10^{-13}	-0.02 (0.003)	7.7×10^{-15}	158496502-158518238 (21,737)	7	46%
	3‡	rs56188432	chr2:158406865:G:A (0.2%)	*ACVR1C* p.I195T	-0.14 (0.021)	4.9×10^{-11}	-0.14 (0.021)	5.4×10^{-12}	158406865 (1)	1	>99%
Experiment-level p-value analysis†											
FGF1	1	rs10477191	chr5:142077715:A:G (95.1%)	79bp 5' of *FGF1*	-0.04 (0.005)	5.5×10^{-17}	-0.04 (0.005)	7.1×10^{-16}	142077715 (1)	1	>99%
	2	rs7712968	chr5:142086214:T:C (93.3%)	8.6kb 5' of *FGF1*	-0.03 (0.004)	1.3×10^{-12}	-0.03 (0.004)	3.5×10^{-11}	142082930-142101101 (18,172)	5	58%
	3	rs34000	chr5:141973501:T:C	3'-UTR of	0.01	1.2×10^{-10}	0.01	9.9×10^{-08}	141480886-	192	30%

			(59.6%)	*FGF1*	(0.002)		(0.002)		142470008 (989,123)		
	4	rs10065321	chr5:141857415:C:T (58.3%)	114kb 3' of *FGF1*	0.01 (0.002)	1.3×10^{-09}	0.01 (0.002)	3.8×10^{-10}	141857415-141861399 (3,985)	5	55%
	5	rs2434416	chr5:141789701:A:C (56.2%)	85kb 5' of *SPRY4*	-0.01 (0.002)	8.3×10^{-09}	-0.01 (0.002)	1.5×10^{-09}	141769319-141824669 (55,351)	34	22%
	6‡	rs17223632	chr5:141993631:T:C (0.3%)	*FGF1* p.G21E	-0.10 (0.018)	8.1×10^{-08}	-0.09 (0.018)	1.6×10^{-07}	141589594-142413739 (824,146)	62	98%

Analyses are from 450,562 European ancestry individuals. Beta and standard errors are in standardized units of BMI-adjusted WHR per copy of the effect allele. Genomic coordinates according to human genome reference sequence GRCh37.

* Adjusting for conditionally-independent index variants highlighted in the joint conditional model.

† Using a p-value threshold $p<1.3\times10^{-06}$, corresponding to a Bonferroni correction for 37,435 genetic variants studied in this analysis.

Abbreviations: SE, standard error; SD, standard deviation.

‡ Variant identified in the genome-wide scan of rare nonsynonymous variants.

Abbreviations: SE, standard error; SD, standard deviation; PPA, posterior probability of association.

Figure Legends

Figure 1. Regional association plots of the overall and statistically-decomposed signals at the *CALCRL, PLIN1, PDE3B* and *ACVR1C* genes. Plots were drawn using LocusZoom (99). Joint meta-analysis models using GCTA (79) were used at each locus to assess how many independent signals were present. Then, at each locus each signal was statistically-decomposed from others by estimating associations of all variants in the region adjusted for all other index variants at the region. Fine-mapping of each signal was performed using a Bayesian approach (80).

Figure 2. Association of rare nonsynonymous genetic variants at *CALCRL, PLIN1* and *PDE3B* with continuous metabolic traits and risk of cardio-metabolic disease outcomes. Associations are presented as beta coefficient in standardized units of continuous trait or odds ratio for disease outcome per minor allele. The minor allele is listed following the rsid above the corresponding plot. Lipid association estimates were not available for rs150090666 in the Global Lipids Genetics Consortium, so they were estimated in the Fenland, InterAct and EPIC-Norfolk studies. Abbreviations: WHR, waist to hip ratio *unadjusted* for body mass index; Waist, waist circumference; Hip, hip circumference; BMI, body mass index; BF %, body fat percentage; SBP, systolic blood pressure; DBP, diastolic blood pressure; LDL-C, low-density lipoprotein cholesterol; HDL-C, high-density lipoprotein cholesterol; SD, standard deviation; OR, odds ratio.

Figure 3. Associations with continuous metabolic traits and risk of cardio-metabolic disease outcomes of genetic variants at the *ACVR1C* gene. The three genetic variants were independently associated with waist-to-hip ratio adjusted for body mass index in conditional analyses at the *ACVR1C* gene. Associations are presented as beta coefficient in standardized units of continuous trait or odds ratio for disease outcome per minor allele. The minor allele is listed following the rsid above the corresponding plot. Abbreviations: WHR, waist to hip ratio *unadjusted* for body mass index; Waist, waist circumference; Hip, hip circumference; BMI, body mass index; BF %, body *fat* percentage; SBP, systolic blood pressure; DBP, diastolic blood pressure; LDL-C, low-density lipoprotein cholesterol; HDL-C, high-density lipoprotein cholesterol; SD, standard deviation; OR, odds ratio.

Figure 4. Schematic depiction of the three catalytic reactions of intracellular lipolysis and key genes in the pathway. Evidence contributing to this representation has been recently reviewed (46).

Figure 5. Phenotypic associations and functional consequences of the rs140201358-G variant in *PNPLA2*. *Panel A* reports associations with continuous traits of rs140201358-G p.N252K, while ***Panel B*** reports associations with cardio-metabolic disease outcomes. Associations are presented as beta coefficient in standardized units of continuous trait or odds ratio for disease outcome per minor allele G. The minor allele is listed following the rsid above the corresponding plot. Abbreviations: WHR, waist to hip ratio unadjusted for body mass index; Waist, waist circumference; Hip, hip circumference; BMI, body mass index; BF %, body fat percentage; SBP, systolic blood pressure; DBP, diastolic blood pressure; LDL-C, low-density lipoprotein cholesterol; HDL-C, high-density lipoprotein cholesterol; SD, standard deviation; OR, odds ratio. ***Panel C*** shows the specific enzymatic activity of PNPLA2-N252K and wild-type protein in *in vitro* expression studies. The graph reports the results of three technical experimental replicates. Full blue circles (individual replicate result) and horizontal bars (averages) are for wild type PNPLA2 while full dark red circles (individual replicate result) and horizontal bars (averages) are for p.N252K mutant PNPLA2. Abbreviations: FA, fatty acids; ABHD5, Abhydrolase Domain Containing 5 also known as Comparative Gene Identification-58 (CGI-58); G0G2, G0/G1 Switch 2. ***Panel D*** represents the location of the rs140201358 p.N252K variant at the exon 6 – intron 6 splice junction of *PNPLA2*. At the top of the panel is a representation of conservation of residues across mammalian species, with the proportion of observed nucleotides at each position represented by the size of the font. ***Panel E*** shows the results of allele-specific expression of *PNPLA2* in subcutaneous adipose tissue from four unrelated heterozygous carriers of rs140201358 p.N252K. The individual results are shown on the left, while the pooled results on the right. The reported p-values are two-tailed binomial probabilities. ***Panel F*** shows the association of rs140201358 N252K genotype with *PNPLA2* gene expression measured by quantitative transcription polymerase chain reaction in peripheral blood mononuclear cells from 106 homozygous carriers of the wild-type C allele (i.e. 252N) and 26 heterozygous carriers of the alternative G allele (i.e. 252K). The mRNA levels of *PNPLA2* were standardized on the basis of the distribution in homozygous wild-type participants. Boxes represent the median and interquartile range, whiskers represent the upper and lower adjacent values, circles represent outliers for each genotype group. Association between genotype and *PNPLA2* expression was estimated by linear regression.

Figures

Figure 1

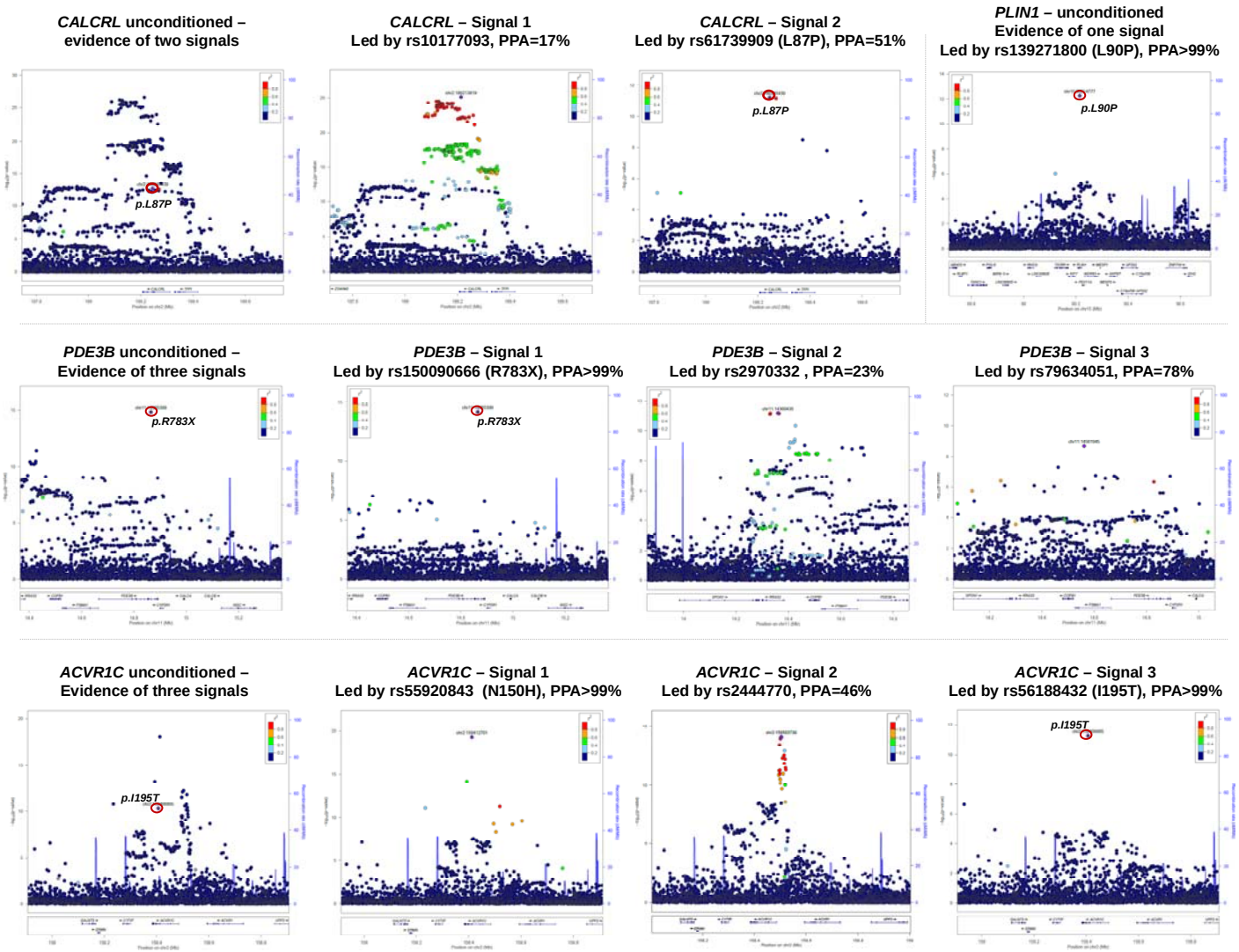

Figure 2

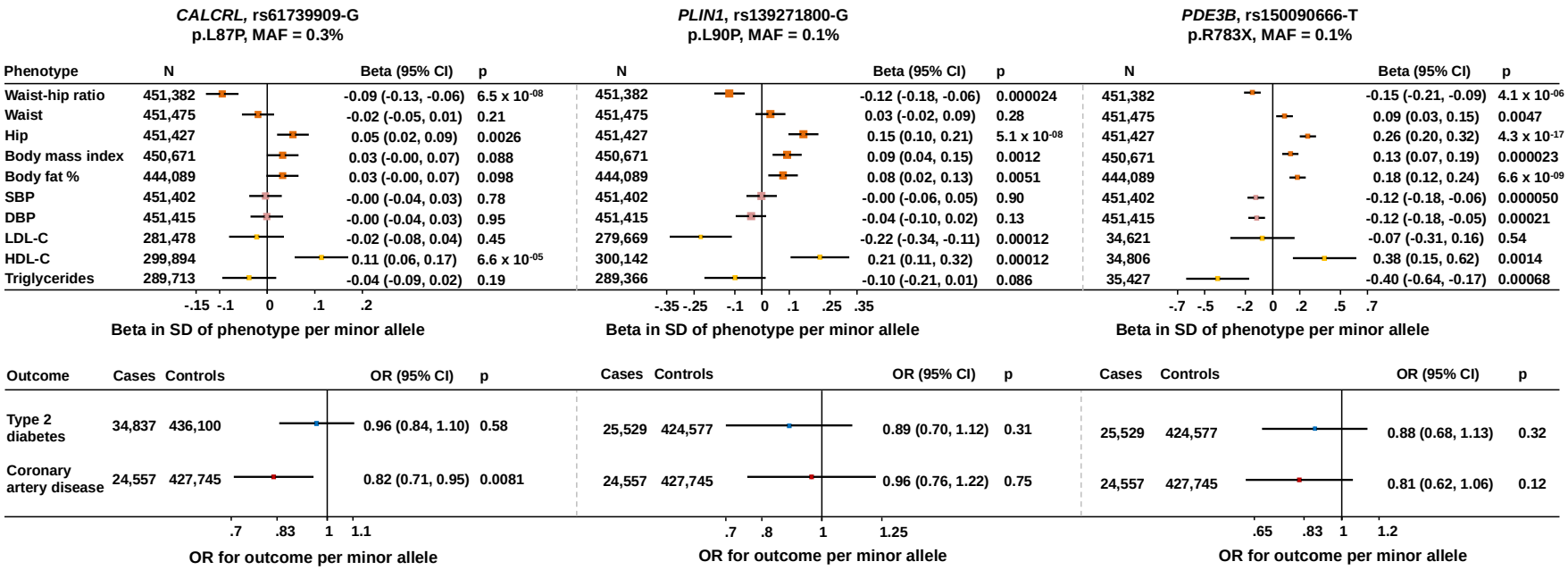

Figure 3

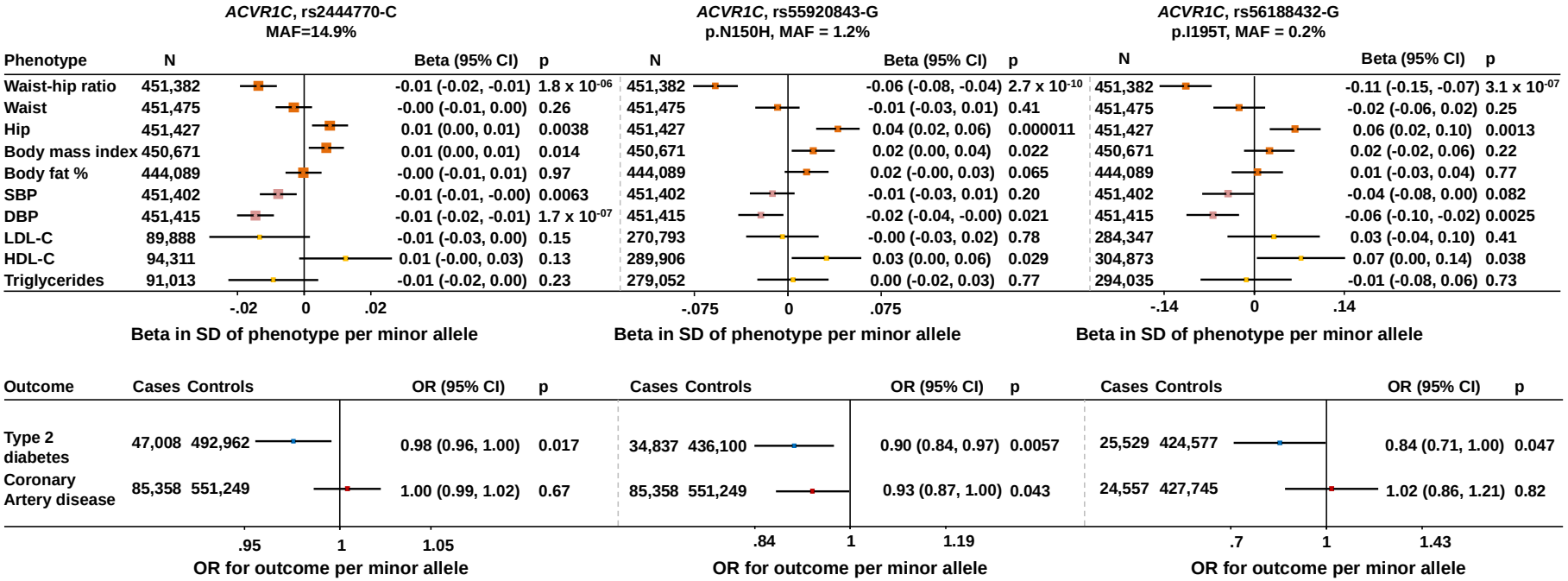

Figure 4

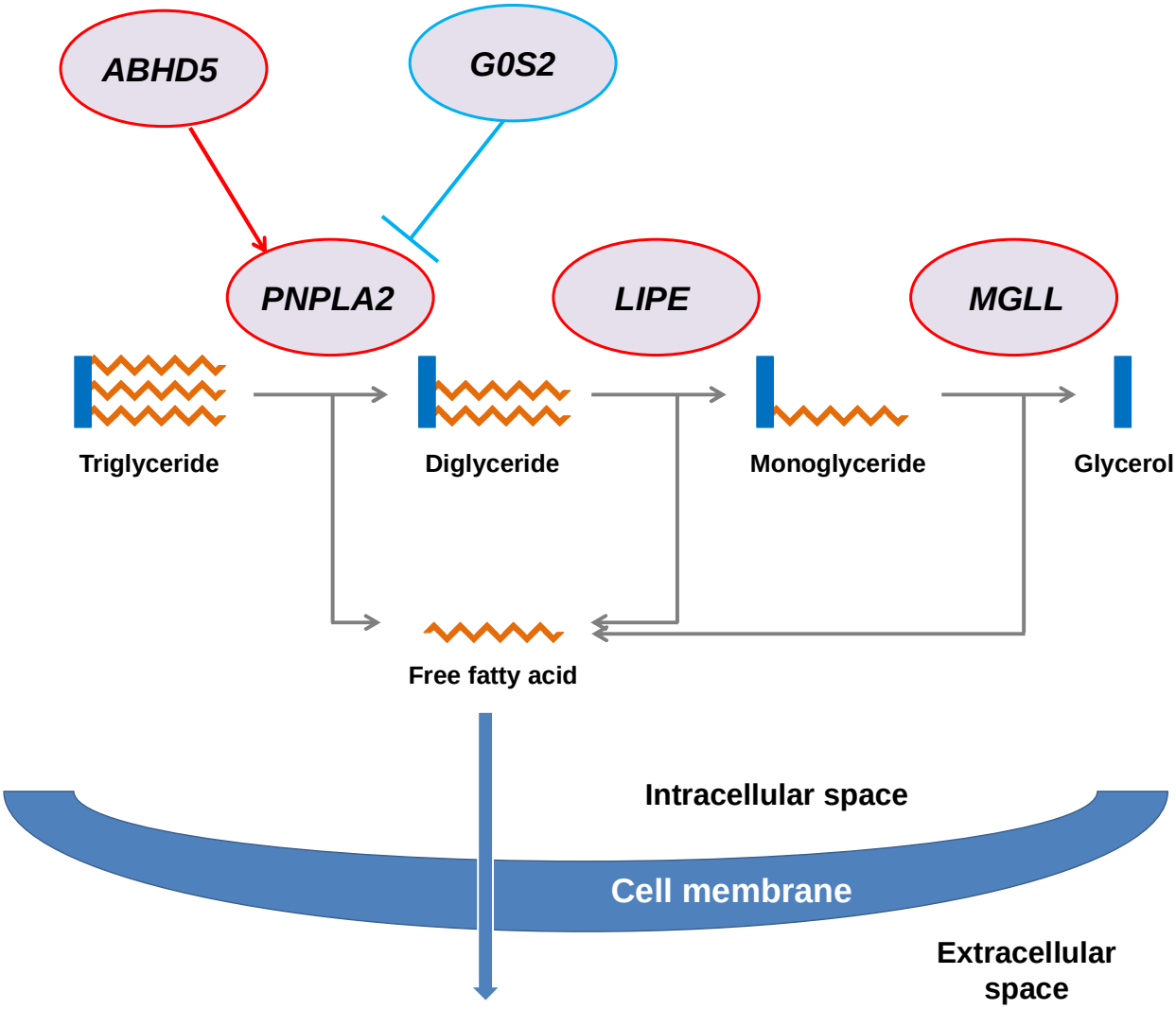

Figure 5

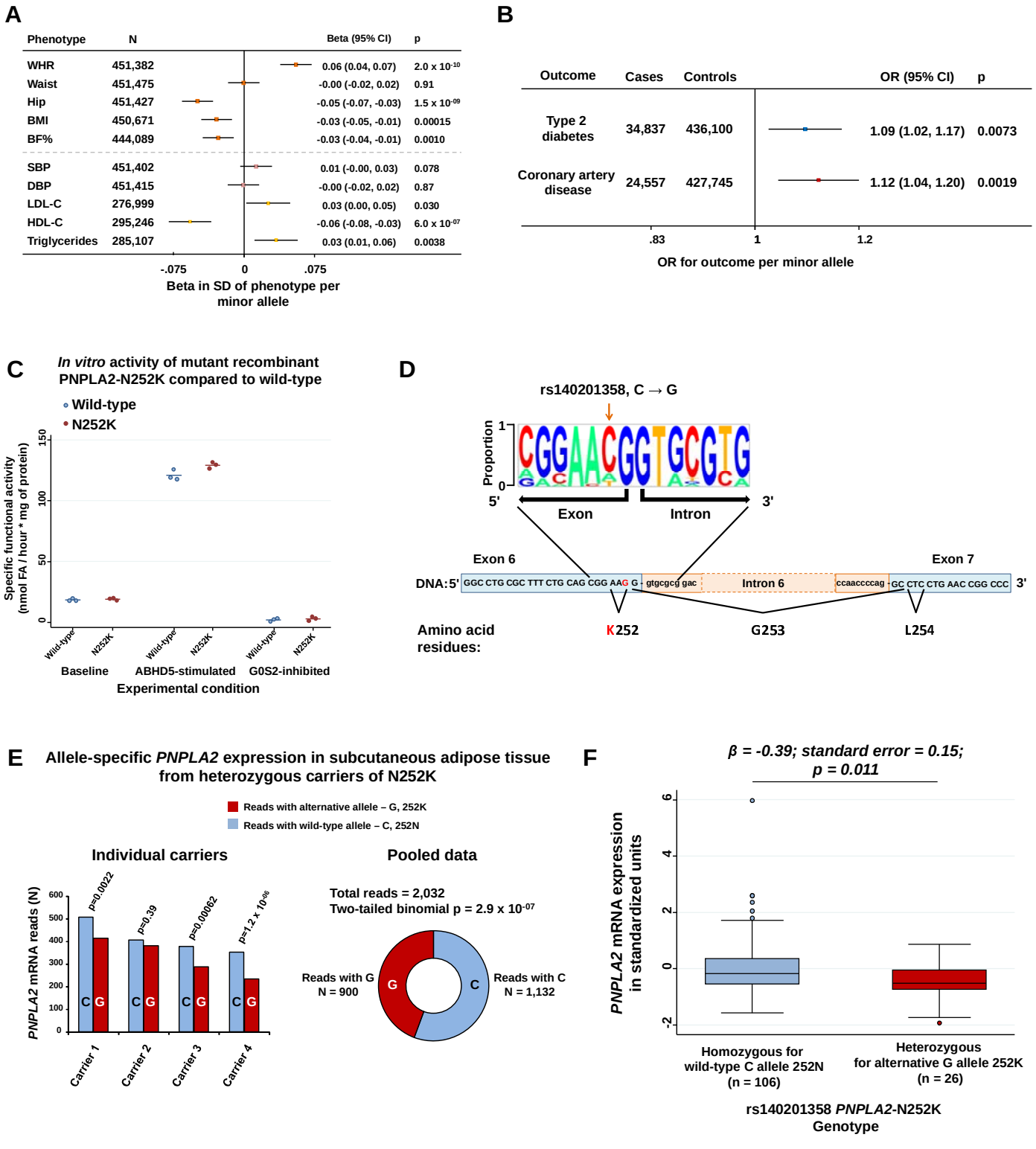

References

1. Dale CE, *et al.* (2017) Causal Associations of Adiposity and Body Fat Distribution With Coronary Heart Disease, Stroke Subtypes, and Type 2 Diabetes Mellitus: A Mendelian Randomization Analysis. *Circulation* 135(24):2373-2388.
2. Emerging Risk Factors C, *et al.* (2011) Separate and combined associations of body-mass index and abdominal adiposity with cardiovascular disease: collaborative analysis of 58 prospective studies. *Lancet* 377(9771):1085-1095.
3. Yusuf S, *et al.* (2005) Obesity and the risk of myocardial infarction in 27,000 participants from 52 countries: a case-control study. *Lancet* 366(9497):1640-1649.
4. Pischon T, *et al.* (2008) General and abdominal adiposity and risk of death in Europe. *The New England journal of medicine* 359(20):2105-2120.
5. Emdin CA, *et al.* (2017) Genetic Association of Waist-to-Hip Ratio With Cardiometabolic Traits, Type 2 Diabetes, and Coronary Heart Disease. *JAMA : the journal of the American Medical Association* 317(6):626-634.
6. Shungin D, *et al.* (2015) New genetic loci link adipose and insulin biology to body fat distribution. *Nature* 518(7538):187-196.
7. Lotta LA, *et al.* (2017) Integrative genomic analysis implicates limited peripheral adipose storage capacity in the pathogenesis of human insulin resistance. *Nature genetics* 49(1):17-26.
8. Chu AY, *et al.* (2017) Multiethnic genome-wide meta-analysis of ectopic fat depots identifies loci associated with adipocyte development and differentiation. *Nature genetics* 49(1):125-130.
9. Cohen JC, Boerwinkle E, Mosley TH, Jr., & Hobbs HH (2006) Sequence variations in PCSK9, low LDL, and protection against coronary heart disease. *The New England journal of medicine* 354(12):1264-1272.
10. Kathiresan S & Myocardial Infarction Genetics C (2008) A PCSK9 missense variant associated with a reduced risk of early-onset myocardial infarction. *The New England journal of medicine* 358(21):2299-2300.
11. Clarke R, *et al.* (2009) Genetic variants associated with Lp(a) lipoprotein level and coronary disease. *The New England journal of medicine* 361(26):2518-2528.
12. Tg, *et al.* (2014) Loss-of-function mutations in APOC3, triglycerides, and coronary disease. *The New England journal of medicine* 371(1):22-31.
13. Jorgensen AB, Frikke-Schmidt R, Nordestgaard BG, & Tybjaerg-Hansen A (2014) Loss-of-function mutations in APOC3 and risk of ischemic vascular disease. *The New England journal of medicine* 371(1):32-41.
14. Musunuru K, *et al.* (2010) Exome sequencing, ANGPTL3 mutations, and familial combined hypolipidemia. *The New England journal of medicine* 363(23):2220-2227.
15. Dewey FE, *et al.* (2017) Genetic and Pharmacologic Inactivation of ANGPTL3 and Cardiovascular Disease. *The New England journal of medicine* 377(3):211-221.
16. Stitziel NO, *et al.* (2017) ANGPTL3 Deficiency and Protection Against Coronary Artery Disease. *Journal of the American College of Cardiology* 69(16):2054-2063.
17. Stein EA, *et al.* (2012) Effect of a monoclonal antibody to PCSK9 on LDL cholesterol. *The New England journal of medicine* 366(12):1108-1118.
18. Gaudet D, *et al.* (2014) Targeting APOC3 in the familial chylomicronemia syndrome. *The New England journal of medicine* 371(23):2200-2206.
19. Gaudet D, *et al.* (2015) Antisense Inhibition of Apolipoprotein C-III in Patients with Hypertriglyceridemia. *The New England journal of medicine* 373(5):438-447.
20. Graham MJ, *et al.* (2017) Cardiovascular and Metabolic Effects of ANGPTL3 Antisense Oligonucleotides. *The New England journal of medicine* 377(3):222-232.
21. Gaudet D, *et al.* (2017) ANGPTL3 Inhibition in Homozygous Familial Hypercholesterolemia. *The New England journal of medicine* 377(3):296-297.

22. Viney NJ, *et al.* (2016) Antisense oligonucleotides targeting apolipoprotein(a) in people with raised lipoprotein(a): two randomised, double-blind, placebo-controlled, dose-ranging trials. *Lancet* 388(10057):2239-2253.
23. Genomes Project C, *et al.* (2012) An integrated map of genetic variation from 1,092 human genomes. *Nature* 491(7422):56-65.
24. McCarthy S, *et al.* (2016) A reference panel of 64,976 haplotypes for genotype imputation. *Nature genetics* 48(10):1279-1283.
25. Raychaudhuri S (2011) Mapping rare and common causal alleles for complex human diseases. *Cell* 147(1):57-69.
26. Emdin CA, *et al.* (2018) Analysis of predicted loss-of-function variants in UK Biobank identifies variants protective for disease. *Nature communications* 9(1):1613.
27. Dackor RT, *et al.* (2006) Hydrops fetalis, cardiovascular defects, and embryonic lethality in mice lacking the calcitonin receptor-like receptor gene. *Molecular and cellular biology* 26(7):2511-2518.
28. Gandotra S, *et al.* (2011) Perilipin deficiency and autosomal dominant partial lipodystrophy. *The New England journal of medicine* 364(8):740-748.
29. DiPilato LM, *et al.* (2015) The Role of PDE3B Phosphorylation in the Inhibition of Lipolysis by Insulin. *Molecular and cellular biology* 35(16):2752-2760.
30. Yogosawa S, Mizutani S, Ogawa Y, & Izumi T (2013) Activin receptor-like kinase 7 suppresses lipolysis to accumulate fat in obesity through downregulation of peroxisome proliferator-activated receptor gamma and C/EBPalpha. *Diabetes* 62(1):115-123.
31. Consortium GT (2015) Human genomics. The Genotype-Tissue Expression (GTEx) pilot analysis: multitissue gene regulation in humans. *Science* 348(6235):648-660.
32. Granneman JG, Moore HP, Krishnamoorthy R, & Rathod M (2009) Perilipin controls lipolysis by regulating the interactions of AB-hydrolase containing 5 (Abhd5) and adipose triglyceride lipase (Atgl). *The Journal of biological chemistry* 284(50):34538-34544.
33. Gandotra S, *et al.* (2011) Human frame shift mutations affecting the carboxyl terminus of perilipin increase lipolysis by failing to sequester the adipose triglyceride lipase (ATGL) coactivator AB-hydrolase-containing 5 (ABHD5). *The Journal of biological chemistry* 286(40):34998-35006.
34. Degerman E, *et al.* (2011) From PDE3B to the regulation of energy homeostasis. *Current opinion in pharmacology* 11(6):676-682.
35. Dong Y, Betancourt A, Belfort M, & Yallampalli C (2017) Targeting Adrenomedullin to Improve Lipid Homeostasis in Diabetic Pregnancies. *The Journal of clinical endocrinology and metabolism* 102(9):3425-3436.
36. Semple RK, Savage DB, Cochran EK, Gorden P, & O'Rahilly S (2011) Genetic syndromes of severe insulin resistance. *Endocrine reviews* 32(4):498-514.
37. Zimmermann R, *et al.* (2004) Fat mobilization in adipose tissue is promoted by adipose triglyceride lipase. *Science* 306(5700):1383-1386.
38. Sveinbjornsson G, *et al.* (2016) Weighting sequence variants based on their annotation increases power of whole-genome association studies. *Nature genetics* 48(3):314-317.
39. Garg A (2004) Acquired and inherited lipodystrophies. *The New England journal of medicine* 350(12):1220-1234.
40. Ryden M, Andersson DP, Bergstrom IB, & Arner P (2014) Adipose tissue and metabolic alterations: regional differences in fat cell size and number matter, but differently: a cross-sectional study. *The Journal of clinical endocrinology and metabolism* 99(10):E1870-1876.
41. Karpe F & Pinnick KE (2015) Biology of upper-body and lower-body adipose tissue--link to whole-body phenotypes. *Nature reviews. Endocrinology* 11(2):90-100.
42. Gavrilova O, *et al.* (2000) Surgical implantation of adipose tissue reverses diabetes in lipoatrophic mice. *The Journal of clinical investigation* 105(3):271-278.
43. Scott RA, *et al.* (2014) Common genetic variants highlight the role of insulin resistance and body fat distribution in type 2 diabetes, independent of obesity. *Diabetes* 63(12):4378-4387.

44. Yaghootkar H, *et al.* (2014) Genetic evidence for a normal-weight "metabolically obese" phenotype linking insulin resistance, hypertension, coronary artery disease, and type 2 diabetes. *Diabetes* 63(12):4369-4377.
45. Yaghootkar H, *et al.* (2016) Genetic evidence for a link between favorable adiposity and lower risk of type 2 diabetes, hypertension and heart disease. *Diabetes*.
46. Zechner R, Madeo F, & Kratky D (2017) Cytosolic lipolysis and lipophagy: two sides of the same coin. *Nature reviews. Molecular cell biology* 18(11):671-684.
47. Arner P, *et al.* (2011) Dynamics of human adipose lipid turnover in health and metabolic disease. *Nature* 478(7367):110-113.
48. Jonker JW, *et al.* (2012) A PPARgamma-FGF1 axis is required for adaptive adipose remodelling and metabolic homeostasis. *Nature* 485(7398):391-394.
49. Fischer J, *et al.* (2007) The gene encoding adipose triglyceride lipase (PNPLA2) is mutated in neutral lipid storage disease with myopathy. *Nature genetics* 39(1):28-30.
50. Pennisi EM, *et al.* (2017) Neutral Lipid Storage Diseases: clinical/genetic features and natural history in a large cohort of Italian patients. *Orphanet journal of rare diseases* 12(1):90.
51. Reilich P, *et al.* (2011) The phenotypic spectrum of neutral lipid storage myopathy due to mutations in the PNPLA2 gene. *Journal of neurology* 258(11):1987-1997.
52. Kaneko K, *et al.* (2014) A novel mutation in PNPLA2 causes neutral lipid storage disease with myopathy and triglyceride deposit cardiomyovasculopathy: a case report and literature review. *Neuromuscular disorders : NMD* 24(7):634-641.
53. Albert JS, *et al.* (2014) Null mutation in hormone-sensitive lipase gene and risk of type 2 diabetes. *The New England journal of medicine* 370(24):2307-2315.
54. Schweiger M, *et al.* (2017) Pharmacological inhibition of adipose triglyceride lipase corrects high-fat diet-induced insulin resistance and hepatosteatosis in mice. *Nature communications* 8:14859.
55. Mayer N, *et al.* (2013) Development of small-molecule inhibitors targeting adipose triglyceride lipase. *Nature chemical biology* 9(12):785-787.
56. Cerk IK, *et al.* (2014) A peptide derived from G0/G1 switch gene 2 acts as noncompetitive inhibitor of adipose triglyceride lipase. *The Journal of biological chemistry* 289(47):32559-32570.
57. Cain C (2014) ALK7's obese functions. *SciBX* 7.
58. Bedenis R, *et al.* (2014) Cilostazol for intermittent claudication. *The Cochrane database of systematic reviews* (10):CD003748.
59. Tan L, *et al.* (2015) Efficacy and Safety of Cilostazol Therapy in Ischemic Stroke: A Meta-analysis. *Journal of stroke and cerebrovascular diseases : the official journal of National Stroke Association* 24(5):930-938.
60. Rondini EA, *et al.* (2017) Novel Pharmacological Probes Reveal ABHD5 as a Locus of Lipolysis Control in White and Brown Adipocytes. *The Journal of pharmacology and experimental therapeutics* 363(3):367-376.
61. Suh JM, *et al.* (2014) Endocrinization of FGF1 produces a neomorphic and potent insulin sensitizer. *Nature* 513(7518):436-439.
62. Gasser E, Moutos CP, Downes M, & Evans RM (2017) FGF1 - a new weapon to control type 2 diabetes mellitus. *Nature reviews. Endocrinology* 13(10):599-609.
63. Sudlow C, *et al.* (2015) UK biobank: an open access resource for identifying the causes of a wide range of complex diseases of middle and old age. *PLoS medicine* 12(3):e1001779.
64. Mahajan A, *et al.* (2017) Refining The Accuracy Of Validated Target Identification Through Coding Variant Fine-Mapping In Type 2 Diabetes. *bioRxiv*.
65. Eastwood SV, *et al.* (2016) Algorithms for the Capture and Adjudication of Prevalent and Incident Diabetes in UK Biobank. *PloS one* 11(9):e0162388.
66. Klarin D, *et al.* (2017) Genetic analysis in UK Biobank links insulin resistance and transendothelial migration pathways to coronary artery disease. *Nature genetics*.

67. Nelson CP, *et al.* (2017) Association analyses based on false discovery rate implicate new loci for coronary artery disease. *Nature genetics*.
68. InterAct C, *et al.* (2011) Design and cohort description of the InterAct Project: an examination of the interaction of genetic and lifestyle factors on the incidence of type 2 diabetes in the EPIC Study. *Diabetologia* 54(9):2272-2282.
69. Morris AP, *et al.* (2012) Large-scale association analysis provides insights into the genetic architecture and pathophysiology of type 2 diabetes. *Nature genetics* 44(9):981-990.
70. Nikpay M, *et al.* (2015) A comprehensive 1,000 Genomes-based genome-wide association meta-analysis of coronary artery disease. *Nature genetics* 47(10):1121-1130.
71. Global Lipids Genetics C, *et al.* (2013) Discovery and refinement of loci associated with lipid levels. *Nature genetics* 45(11):1274-1283.
72. Liu DJ, *et al.* (2017) Exome-wide association study of plasma lipids in >300,000 individuals. *Nature genetics*.
73. Lotta LA, *et al.* (2016) Genetic Predisposition to an Impaired Metabolism of the Branched-Chain Amino Acids and Risk of Type 2 Diabetes: A Mendelian Randomisation Analysis. *PLoS medicine* 13(11):e1002179.
74. Day N, *et al.* (1999) EPIC-Norfolk: study design and characteristics of the cohort. European Prospective Investigation of Cancer. *British journal of cancer* 80 Suppl 1:95-103.
75. Aschard H, Vilhjalmsson BJ, Joshi AD, Price AL, & Kraft P (2015) Adjusting for heritable covariates can bias effect estimates in genome-wide association studies. *American journal of human genetics* 96(2):329-339.
76. Bycroft C, *et al.* (2017) Genome-wide genetic data on ~500,000 UK Biobank participants. *bioRxiv*.
77. Wang K, Li M, & Hakonarson H (2010) ANNOVAR: functional annotation of genetic variants from high-throughput sequencing data. *Nucleic acids research* 38(16):e164.
78. Loh PR, *et al.* (2015) Efficient Bayesian mixed-model analysis increases association power in large cohorts. *Nature genetics* 47(3):284-290.
79. Yang J, Lee SH, Goddard ME, & Visscher PM (2011) GCTA: a tool for genome-wide complex trait analysis. *American journal of human genetics* 88(1):76-82.
80. Wellcome Trust Case Control C, *et al.* (2012) Bayesian refinement of association signals for 14 loci in 3 common diseases. *Nature genetics* 44(12):1294-1301.
81. Webb B & Sali A (2016) Comparative Protein Structure Modeling Using MODELLER. *Current protocols in protein science* 86:2 9 1-2 9 37.
82. Alva V, Nam SZ, Soding J, & Lupas AN (2016) The MPI bioinformatics Toolkit as an integrative platform for advanced protein sequence and structure analysis. *Nucleic acids research* 44(W1):W410-415.
83. Altenhoff AM, *et al.* (2015) The OMA orthology database in 2015: function predictions, better plant support, synteny view and other improvements. *Nucleic acids research* 43(Database issue):D240-249.
84. Waterhouse AM, Procter JB, Martin DM, Clamp M, & Barton GJ (2009) Jalview Version 2--a multiple sequence alignment editor and analysis workbench. *Bioinformatics* 25(9):1189-1191.
85. Herwig R, Hardt C, Lienhard M, & Kamburov A (2016) Analyzing and interpreting genome data at the network level with ConsensusPathDB. *Nature protocols* 11(10):1889-1907.
86. Coassin S, *et al.* (2010) Investigation and functional characterization of rare genetic variants in the adipose triglyceride lipase in a large healthy working population. *PLoS genetics* 6(12):e1001239.
87. Schweiger M, *et al.* (2014) Measurement of lipolysis. *Methods in enzymology* 538:171-193.
88. Desmet FO, *et al.* (2009) Human Splicing Finder: an online bioinformatics tool to predict splicing signals. *Nucleic acids research* 37(9):e67.
89. Raponi M, *et al.* (2011) Prediction of single-nucleotide substitutions that result in exon skipping: identification of a splicing silencer in BRCA1 exon 6. *Human mutation* 32(4):436-444.

90. Consortium UK, *et al.* (2015) The UK10K project identifies rare variants in health and disease. *Nature* 526(7571):82-90.
91. Buil A, *et al.* (2015) Gene-gene and gene-environment interactions detected by transcriptome sequence analysis in twins. *Nature genetics* 47(1):88-91.
92. Rozowsky J, *et al.* (2011) AlleleSeq: analysis of allele-specific expression and binding in a network framework. *Molecular systems biology* 7:522.
93. Martin M (2011) Cutadapt removes adapter sequences from high-throughput sequencing reads. *EMBnet.journal* 17(1).
94. Schmieder R & Edwards R (2011) Quality control and preprocessing of metagenomic datasets. *Bioinformatics* 27(6):863-864.
95. Dobin A, *et al.* (2013) STAR: ultrafast universal RNA-seq aligner. *Bioinformatics* 29(1):15-21.
96. Zhao H, *et al.* (2014) CrossMap: a versatile tool for coordinate conversion between genome assemblies. *Bioinformatics* 30(7):1006-1007.
97. McKenna A, *et al.* (2010) The Genome Analysis Toolkit: a MapReduce framework for analyzing next-generation DNA sequencing data. *Genome research* 20(9):1297-1303.
98. Burgess S, Butterworth A, & Thompson SG (2013) Mendelian randomization analysis with multiple genetic variants using summarized data. *Genetic epidemiology* 37(7):658-665.
99. Pruim RJ, *et al.* (2010) LocusZoom: regional visualization of genome-wide association scan results. *Bioinformatics* 26(18):2336-2337.